Canonical Wnt signaling exerts bidirectional control on choroid plexus epithelial development

Arpan Parichha*[1], Varun Suresh*[1], Mallika Chatterjee[1$], Aditya Kshirsagar[2], Lihi Ben-Reuven[2], Tsviya Olender[2], M. Mark Taketo[3], Velena Radosevic[4,5], Mihaela Bobic-Rasonja[4,5], Sara Trnski[4], Nataša Jovanov Milošević[#4,5], Orly Reiner[#2], Shubha Tole[#1]

[1]Department of Biological Sciences, Tata Institute of Fundamental Research, Mumbai 400005, India; [2]Department of Molecular Genetics, Weizmann Institute of Science, Israel; [3]Division of Experimental Therapeutics Graduate School of Medicine, Kyoto University (Yoshida-Konoé-Cho, Sakyo), Kyoto 606-8501, Japan; [4]Croatian Institute for Brain Research, Department of Medical Biology, School of Medicine University of Zagreb, Šalata 12, Zagreb, Croatia, [5]University Hospital Centre Zagreb, Department of Gynecology and Department of Pathology and Cytology, Petrova 13, Zagreb, Croatia

*These authors contributed equally to this work

[#]Authors for correspondence: stole@tifr.res.in; orly.reiner@weizmann.ac.il; njovanov@gmail.com

[$]Current address: Amity Institute of Neuropsychology and Neurosciences, Amity University, Noida, India.

Abstract

The choroid plexus (CP) secretes cerebrospinal fluid and is critical for the development and function of the brain. In the telencephalon, the CP epithelium (CPe) arises from the *Wnt*- and *Bmp*- expressing cortical hem. We examined the role of canonical Wnt signaling in CPe development and report that the mouse and human embryonic CPe expresses molecules in this pathway. Either loss of function or constitutive activation of β-catenin, a key mediator of canonical Wnt signaling, causes a profound disruption of mouse CPe development. Loss of β-catenin results in a dysmorphic CPe, while constitutive activation of β-catenin causes a loss of CPe identity and a transformation of this tissue to a hippocampal-like identity. Aspects of this phenomenon are recapitulated in human embryonic stem cell (hESC)-derived organoids. Our results indicate that canonical Wnt signaling is required in a precisely regulated manner for normal CP development in the mammalian brain.

Introduction

The Choroid plexus (CP) produces cerebrospinal fluid (CSF) which plays an important role in the developing and adult brain. The CSF provides protective functions such as cushioning against mechanical damage; nutritive functions; and also signaling functions, providing molecular cues for the developing brain (Johansson, 2014; Lun, et al., 2015). The CP separates the blood from the CSF, creating a checkpoint for regulating the entry and exit of factors (Zappaterra and Lehtinen, 2012; Lun et al., 2015). The CP is also the gateway for immune cells entering or exiting the brain (Meeker et al., 2012).

The CP epithelium (CPe) arises from adjacent neuroepithelial tissue in the telencephalon, diencephalon, and the hindbrain. In the telencephalon, the non-neuronal CPe as well as a sub-population of Cajal-Retzius (CR) neurons arise from the cortical hem (Yoshida et al., 2006; Louvi et al., 2007; Gu *et al.*, 2011). This midline telencephalic signaling center expresses genes that belong to the BMP and WNT families in mouse (Grove et al., 1998) and human (Abu-Khalil et al., 2004). In the marsupial *Monodelphis Domestica,* BrdU positive cells arise from the hem and populate the growing telencephalic CPe in a “conveyor belt” like manner (Liddelow *et al.*, 2010). Consistent with this model, when the size of the cortical hem increases (Monuki et al., 2001), decreases (Konno *et al.*, 2012) or is missing altogether (Grove et al., 1998), there is a parallel change in the extent of the CP.

The mechanisms that regulate the specification of the CPe are important from a developmental, disease, and evolutionary perspective. Obvious candidates for the control of CPe development are the signaling molecules expressed in the neuroepithelial progenitor domains. The hem expresses several members of the Bmp and Wnt families (Furuta et al., 1997; Grove et al., 1998). Of particular interest are mechanisms that govern the decision between the neuronal (Cajal-Retzius cells) versus non-neuronal (CPe) lineages arising from progenitors in the hem.

Bmp signaling is critical for CPe specification: the CP is missing in the *BmpR1a* null mutant mouse (Hebert *et al.*, 2002; Watanabe *et al.*, 2012), and *Bmp4* is sufficient for CPe induction *in vitro* (Eiraku et al., 2008; Watanabe et al., 2012). The role of hem-derived Wnt ligands in CPe development appears to be equally important, though well explored. Non-canonical Wnt5a, expressed in the hem, appears to be required for maintaining the size and the cytoarchitecture of the CPe (Langford et al., 2020). A role for canonical Wnt signaling in CPe development is indicated by the observation that the addition of WNT3a augments the CPe-inducing ability of BMP4 in three-dimensional aggregation culture derived from embryonic stem cells (ESCs). How the CPe responds to canonical Wnt signaling, and whether this pathway

53 is required for CPe development, is an open question, and the focus of this study. We
54 demonstrate that molecules downstream of canonical Wnt signaling are expressed *in vivo* at
55 embryonic stages in mouse and human CPe. Loss of β-catenin, a key member of the canonical
56 Wnt pathway transcriptional complex, results in a dysmorphic CP in the mouse, whereas
57 constitutive activation of β-CATENIN, or treatment with a canonical Wnt agonist of human ESC
58 (hESC)- derived organoids, results in a loss of CPe identity. Together, our results indicate that a
59 precise balance of canonical Wnt signaling is critical for CPe specification and morphogenesis,
60 and that this mechanism for CPe regulation appears to be conserved in humans and rodents.

Results

Canonical Wnt signaling is necessary for normal CP development in mice

We examined whether the molecular machinery required for processing canonical Wnt signaling is present in the developing CPe. The hem and the CPe are identified by the expression of *Wnt3a* and the thyroid hormone T4 carrier transthyretin (*Ttr*), respectively. Several molecules involved in the canonical Wnt signaling pathway, including a receptor, *Frizzled 1* (*Fzd1*), transcriptional regulators β-CATENIN and LEF1*,* as well as a target gene *Axin2,* are each expressed in the CPe at E12.5 and E14.5 in mice (Figure 1A, B). These data suggest that the embryonic CPe has the capability of processing canonical Wnt signaling. *Lmx1a* is expressed in the hem and the CPe (Chizikov and Millen., 2004). To genetically manipulate the developing Cpe we used the Lmx1aCre line which faithfully labels the hem lineage comprising of Cajal-Retzius cells and CPe cells, when crossed to the Ai9 reporter line (Figure 1A).

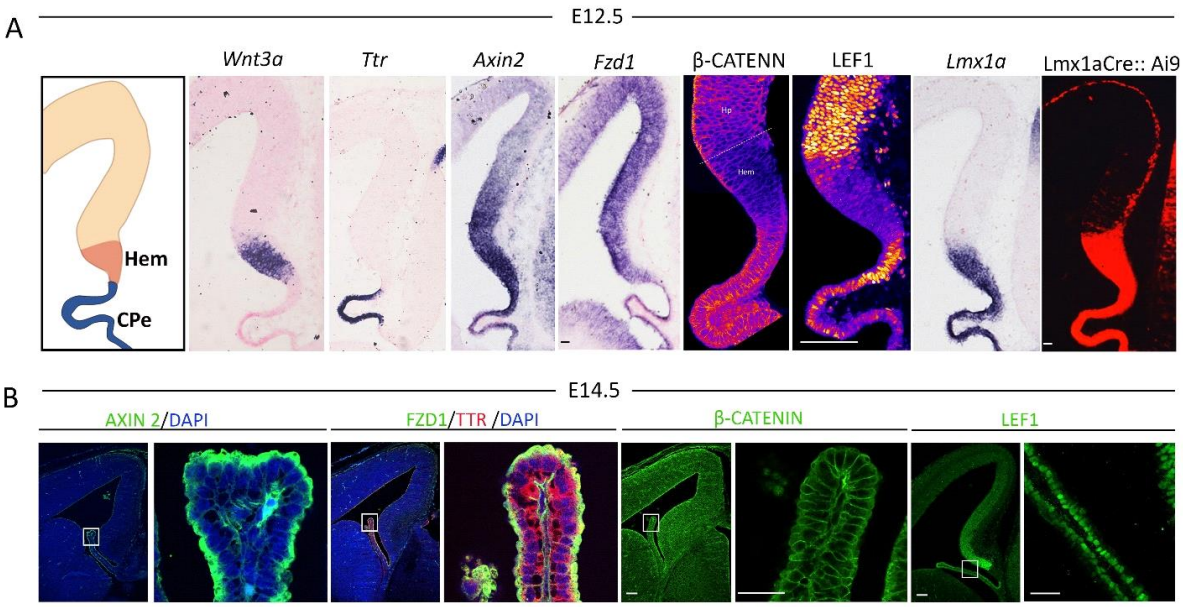

Figure 1. Canonical Wnt signaling components are expressed in the developing mouse choroid plexus epithelium. (A) *In situ* hybridization (*Wnt3a, Ttr*, *Axin2*, *Fzd1*) and immunohistochemistry (β-CATENIN and LEF1) reveal the expression of canonical Wnt signaling components in E12.5 mouse brain sections. *Lmx1a* is expressed in the hem and the CPe. Lmx1a Cre drives the expression of the Ai9 reporter in these tissues and in the hem-derived Cajal-Retzius cells. (B) Immunohistochemistry reveals the expression of AXIN2, FZD1, β-CATENIN, and LEF1 in the E14.5 mouse CPe. All scale bars are 50 μm.

87 We tested whether the CPe requires β-CATENIN function by using a conditional mouse
88 line in which loxP sites flanking exon 2 and 6 of the *ß-catenin* gene (Brault et al., 2001). Cre-
89 mediated recombination results in the removal of a portion of the armadillo repeat encoding
90 segment, resulting in a non-functional protein (loss of function, LOF). We used Lmx1aCre to
91 specifically disrupt *ß-catenin* in the hem and CPe. In the Lmx1aCre:: β-catenin LOF
92 telencephalon, the CP appears dysmorphic and disorganized (Figure 2). From E14.5, some
93 regions of the CP lose their characteristic ribbon-like appearance and fail to express the
94 transcription factor *Otx2*, which is required for CP specification (Johansson et al. 2013), or
95 *Aquaporin 1 (Aqp1)*, a channel critical for CSF production (Kim and Jung 2012; Castañeyra-Ruiz
96 et al. 2016). Though TTR expression appears relatively unaffected, the expression of E-
97 CADHERIN is perturbed, consistent with the abnormally folded appearance of the CP. This
98 disruption of the CP does not ameliorate with time, and at birth, TTR and E-CADHERIN
99 expression reveals an abnormally organized CP (Figure 2). In summary, loss of β-CATENIN
100 function causes profound molecular and cellular perturbations in the CP during its
101 development, demonstrating the requirement for the canonical Wnt pathway in early CP
102 development.

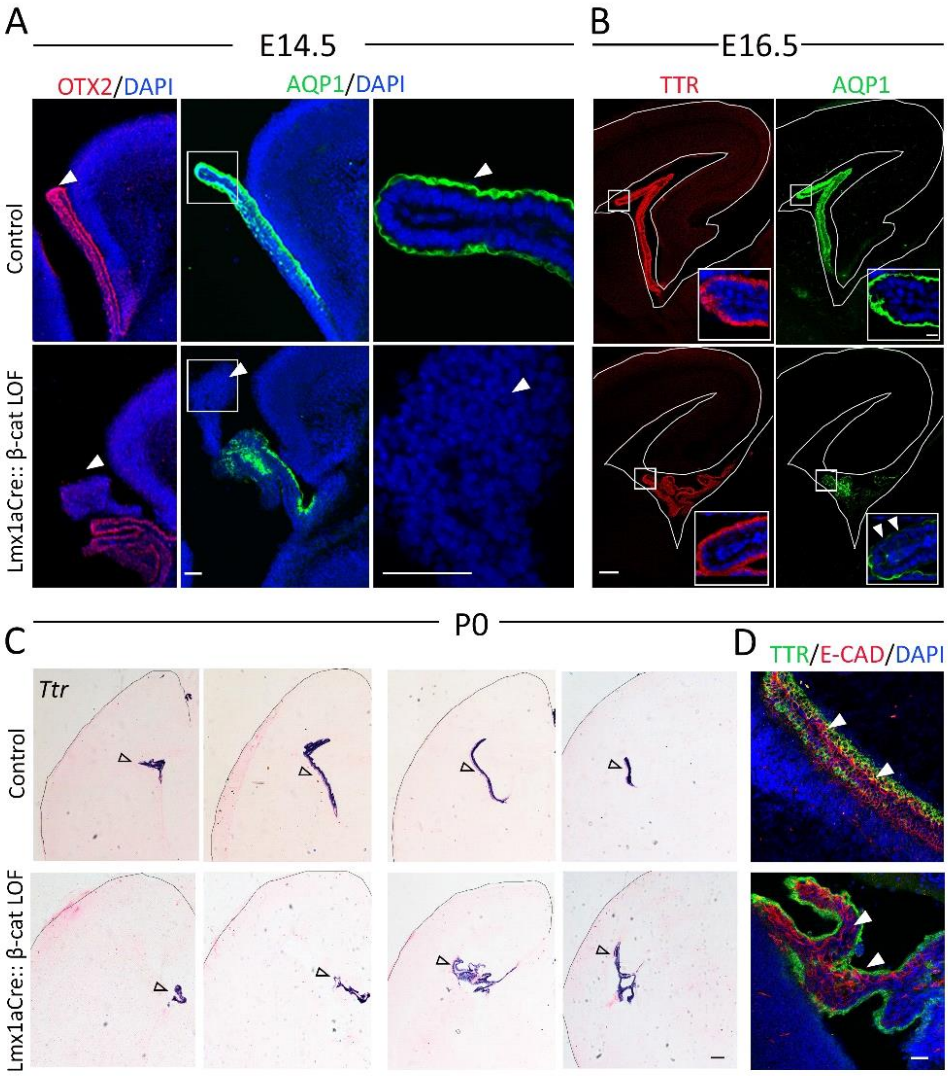

Figure 2. Loss of canonical Wnt signaling (β-catenin LOF) in the hem and CPe disrupts choroid plexus development. (A) OTX2 and AQP1 are expressed throughout the control mouse CP, but are missing in the distal tip of the Lmx1aCre:: β-catenin LOF CP at E14.5 (arrowheads). (B, C) TTR (E16.5 and P0) expression reveals a dysmorphic CP in Lmx1aCre:: β-catenin LOF embryos compared with controls (arrowheads). (B, D) The expression of AQP1 (E16.5) and adherens junction marker E-CADHERIN is uniform in the control CP, but irregular in the Lmx1aCre:: β-catenin LOF CP (arrowheads). All scale bars are 50 μm.

118 **Constitutively active β-catenin disrupts CPe development**

119

120 To examine the effects of constitutive and persistent activation of canonical Wnt
121 signaling in the CPe, we used a mouse line in which exon 3 is flanked by loxP sites. Cre-
122 mediated recombination results in a deletion of a domain that regulates β-CATENIN stability
123 (Harada et al., 1999). The recombined β-catenin allele encodes a protein that remains
124 constitutively active (gain of function, GOF). Analysis of sections from Lmx1aCre:: β-catenin GOF
125 embryos reveal a progressive loss of *Ttr* expression from E12.5, and the CP loses its ribbon-like
126 shape (Figure 3A). LEF1 expression is induced in the CP from E12.5, reflecting the enhanced
127 canonical Wnt signaling as a result of β-catenin GOF. By E15.5, Aqp1 expression is not
128 detectable, and the ventricles are collapsed, possibly due to a lack of fluid resulting from
129 reduced AQP1 expression. E-CADHERIN staining in the Lmx1aCre:: β-catenin GOF CP appears
130 disorganized, consistent with an overall disruption of CP differentiation and morphogenesis
131 (Figure 3B).

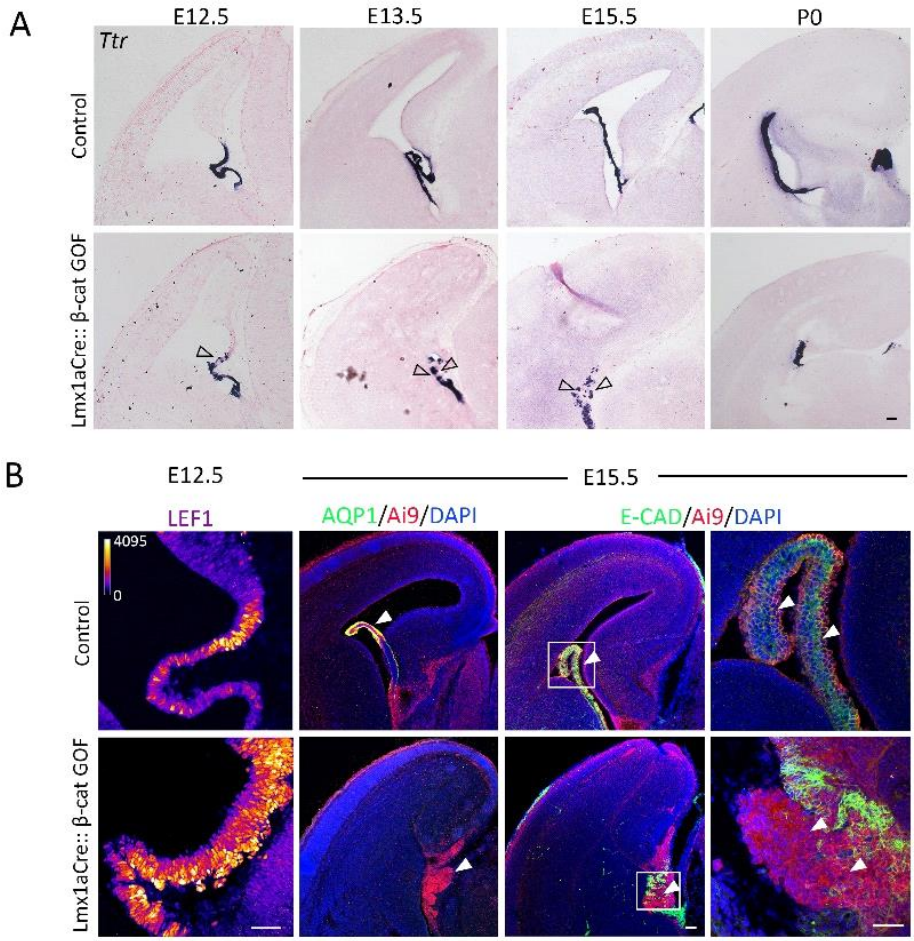

132
133
134
135

Figure 3: Constitutively active β-catenin in the hem and CPe disrupts choroid plexus differentiation and morphogenesis (A) *In situ* hybridization for *Ttr* from E12.5-P0 reveals a patchy expression in Lmx1aCre:: β-catenin GOF brains compared with controls. (B) Immunostaining for LEF1 at E12.5 reveals increased expression at E12.5 consistent with activation of the canonical Wnt pathways in Lmx1aCre:: β-catenin GOF brains. At E15.5, AQP1 expression is lost and E-CADHERIN expression is disorganized in the Lmx1aCre:: β-catenin GOF choroid plexus compared with controls (arrowheads). All scale bars are 50 μm.

Gain of hippocampal-like identity and loss of CPe identity upon constitutive activation of β-catenin

The loss of CPe markers in Lmx1aCre:: β-catenin GOF brains prompted us to examine the identity of the TTR/AQP1-negative tissue. It is well established that canonical Wnt signaling from the cortical hem is necessary and sufficient for the induction of hippocampal fate in adjacent tissue (Lee et al., 200; Machon et al., 2007; Mangale et al., 2008). Therefore, we tested whether neuronal or in particular hippocampal markers were upregulated in the Lmx1aCre:: β-catenin GOF CPe. Indeed, regions devoid of *Ttr* expression displayed expression of the pro-neuronal transcription factor *Neurog2* at E13.5 and E15.5, and also of the dentate gyrus marker *Prox1* (Figure 4A, B). To examine this transformation more comprehensively, we microdissected the CP and hippocampus from E14.5 control and β-catenin GOF embryos and processed these samples for bulk RNA-seq (Figure 4C, D). 2439 genes were downregulated and 2163 genes upregulated in the CP upon constitutive activation of β-catenin, using a 1.5-fold cutoff (p.adj < 0.05; Supplementary Figure 1A). Principal Component Analysis (PCA) and Hierarchical clustering of top 500 genes expressed in the CP and the hippocampus revealed that the overall transcriptome of the Lmx1aCre:: β-catenin GOF CP appears to be more similar to the control hippocampus than the control CP (Figure 4E; Supplementary Figure 1B).

We curated a list of CP-enriched genes (Dani et al., 2019) and found that they were downregulated in the β-catenin GOF CP. In contrast, genes related to hippocampal development and dentate gyrus development (GO:0021766, GO:0021542), including bonafide markers of the developing hippocampus, *Zbtb20,* and *Lhx9*, were upregulated (Supplementary Figure 1. Gene Ontology (GO) analysis of the Differentially Expressed (DE) genes indicated that pathways involved in neurogenesis are upregulated in the β-catenin GOF CP (Supplementary Figure 1). In summary, transcriptomic analysis is consistent with the interpretation that upregulation of canonical Wnt signaling leads to a loss of CPe identity and a transformation to a neuronal/hippocampal-like fate.

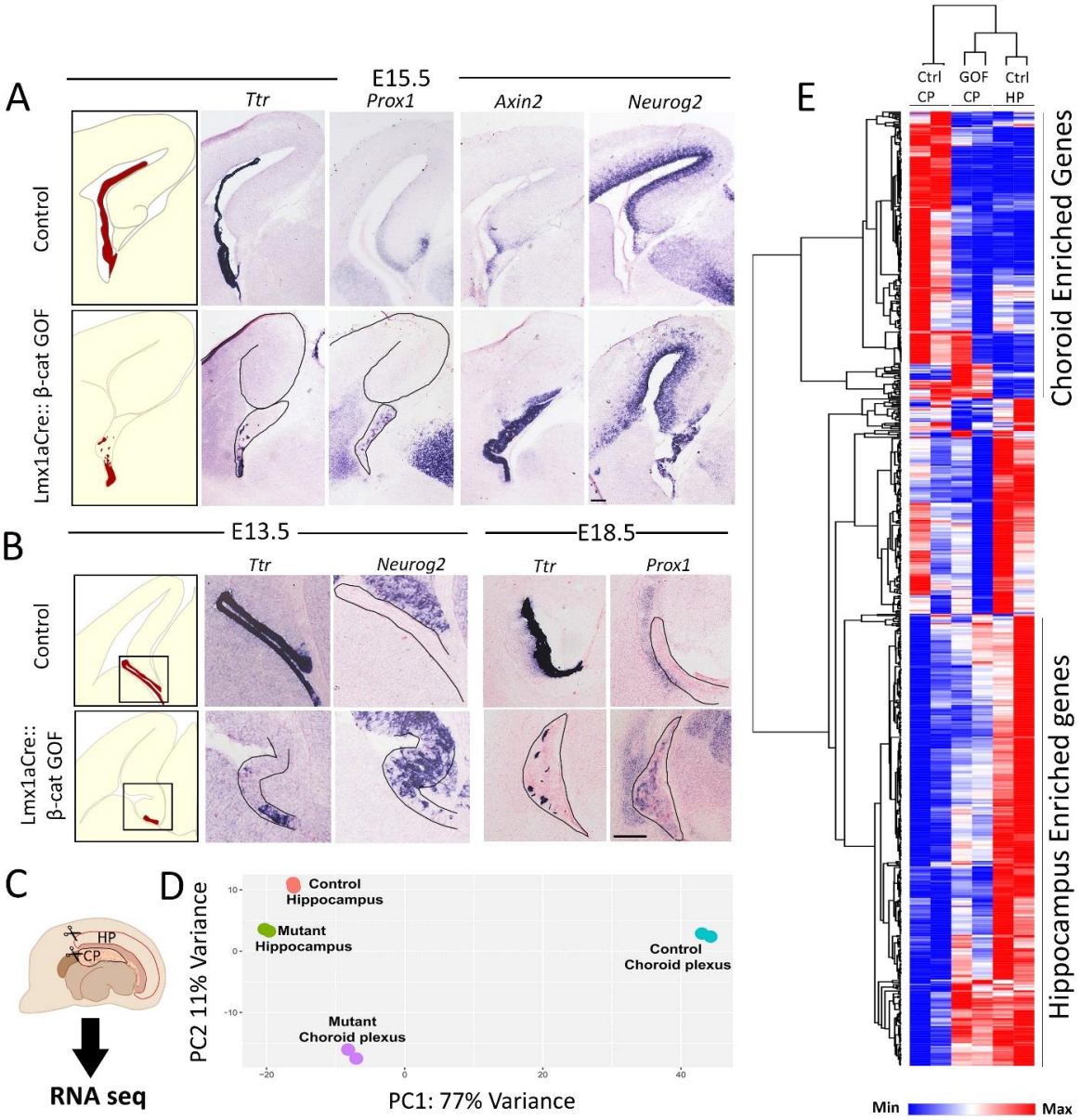

Figure 4. Constitutive activation of β-catenin transforms the CPe to a neuronal and hippocampal-like molecular identity.

(A, B) The Lmx1aCre:: β-catenin GOF CP appears to have lost *Ttr* expression, which is normally seen throughout the control CP at E15.5 (A), E13.5, and E18.5 (B). In contrast, *Prox1*, *Axin2*, and *Neurog2,* which are not expressed in the control CP, are aberrantly expressed in the Lmx1aCre:: β-catenin GOF CP.

(C) A cartoon depicting the dissection of E14.5 mouse CP and hippocampus for RNA-seq analysis. (D) Principal Component Analysis and (E) Heat map of the top 2000 genes plotted as normalized read counts of the RNA-seq data from control and Lmx1aCre:: β-catenin GOF CP and hippocampus. All scale bars are 50 μm.

The human fetal CP displays components of Wnt signaling.

Given the critical role of CSF in brain development and the finding that both β-catenin LOF and GOF disrupt CPe specification and morphogenesis, we sought to explore whether this signaling pathway is important in the development of the human CP. The telencephalic CP develops between gestational weeks 8 to 12 in the human. We collected human fetal samples from GW11 and GW13 and performed immunohistochemical analysis for Wnt signaling components. The human CP is identified by AQP1 and OTX2 expression as well as by its elaborate fan-like morphology in the large ventricles seen in the human embryonic telencephalon (Figure 5). The canonical Wnt receptor, FZD1, is expressed throughout the CPe, as are β-CATENIN, LEF1, and AXIN2 (Figure 5). These findings indicate that canonical Wnt signaling is likely to be active in the human CPe at early stages during CP development.

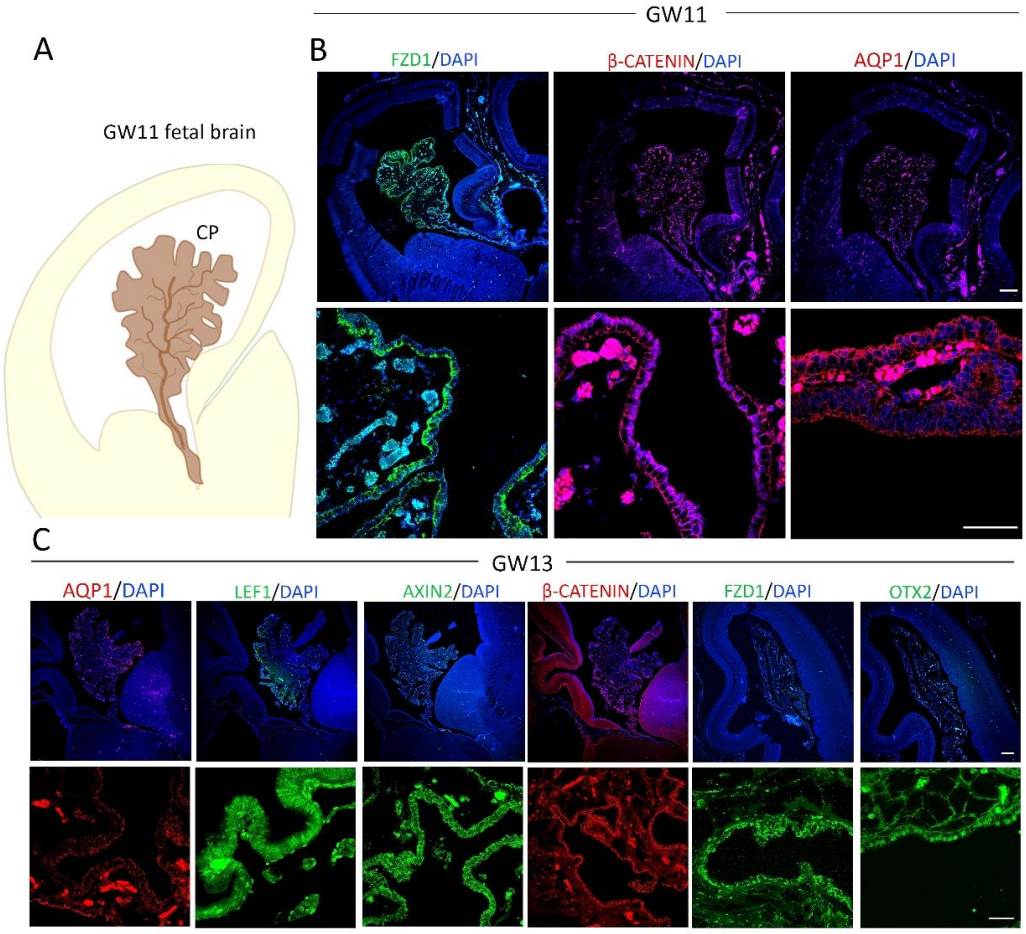

Figure 5: The fetal human CP displays canonical Wnt signaling components
(A) A scheme of the human fetal telencephalic CP (B-C) Immunostaining of human fetal sections at GW11(B) and GW13 (C) for FDZ1, β-CATENIN, AQP1, LEF1, and AXIN 2 reveals the presence of canonical Wnt signaling components and also of the CP marker OTX2. Scale bars are 500 μm (low magnification panels) and 50 μm (high magnification panels) in B and C.

203

204 **CPe-like structures arise in hESC organoids upon a combination of BMP and canonical Wnt**
205 **pathway activation**

206

207 We sought to test whether constitutive activation of canonical Wnt signaling disrupts
208 CPe identity in the human, as it does in the mouse. First, we used established protocols to
209 achieve CPe differentiation in hESC-derived organoids (Sakaguchi et al., 2015). In this protocol,
210 hESCs are aggregated and seeded in a 96 well low-adhesion plate, and over 18 days of
211 incubation, they form spherical structures which grow in diameter (Figure 6A, B). At this stage,
212 the morphogen cocktail containing BMP4 and CHIR, a GSK3 inhibitor, is added. GSK3 is
213 responsible for phosphorylating β-CATENIN and marking it for degradation, so CHIR addition
214 has the effect of creating a constitutively active β-CATENIN (Ying et al., 2008). However, unlike
215 the β-catenin GOF mouse, CHIR can be added in graded amounts to control the extent of
216 canonical Wnt pathway activation (Naujok et al 2014). A cocktail containing a low level of CHIR
217 (3 μM) together with BMP4 (0.5nM) promotes CPe-like differentiation (Sakaguchi et al., 2015).
218 The spherical organoids became slightly tapering and developed multiple protrusions within a
219 few days of exposure to the cocktail (Figure 6B). Immunohistochemistry reveals CPe markers
220 TTR, AQP1, and OTX2 to be expressed along the perimeter of the protrusions, with the cells
221 displaying a cuboidal morphology (Figure 6C, D). To better characterize these organoids, we
222 performed RNA-seq after 12 days of exposure to the cocktail. Even though the CPe-like
223 differentiation was seen only along the perimeter of the organoid, the transcriptomic analysis
224 of the sample revealed characteristic markers of the CPe such as *TTR, AQP1, KRT18, and CLIC6*
225 (Figure 6E). Interestingly, genes associated with the blood-CSF barrier (BCSFB) such as *CLDN3*,
226 *TJP1, TJP2, CDH1*, and *JAM2* were also upregulated, as were several transporters and ion
227 channels encoded by the SLC gene family and genes associated with ciliogenesis, consistent
228 with the ciliated epithelium nature of the CPe (Supplementary Figure 2). In summary, consistent
229 with Sakaguchi et al. (2015), CPe-like structures develop in organoids upon exposure to a
230 cocktail of BMP4 and low levels of CHIR.

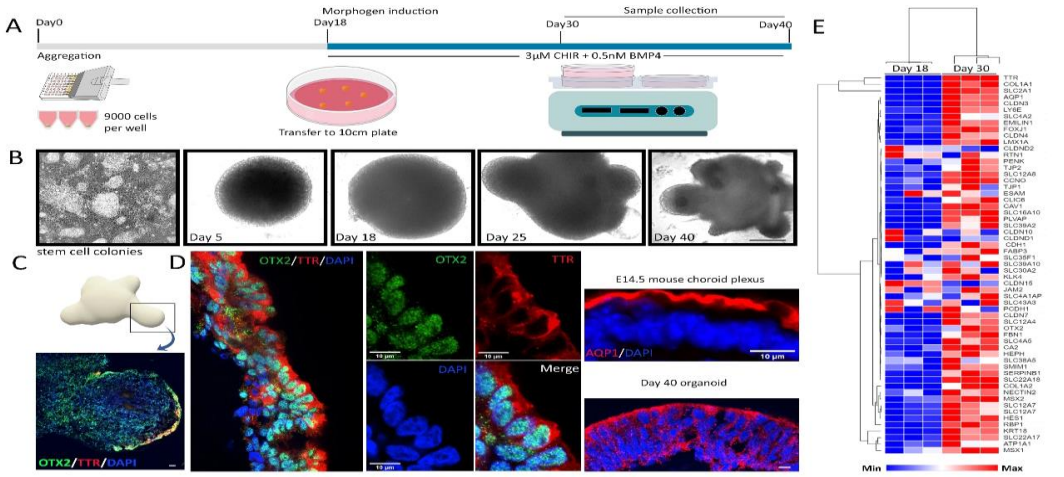

Figure 6: Differentiation of hESC organoid cultures using a CPe differentiation-promoting protocol (A) Schematic presentation describing the organoid culture protocol (B) Bright-field images of organoids at different stages organoid (C, D) Immunostaining reveals the expression of OTX2, TTR, and AQP1 in the perimeter of the protrusions of a day 40 organoid. The AQP1 immunostaining corresponds to that seen in the E14.5 mouse CP. (E) Heat map generated from normalized reads obtained by MARS-Seq shows upregulation of CP-enriched genes by day 30 of the organoid culture. Scale bars are 200 μm in (B), 100 μm in (C), and 10 μm in (D).

Loss of CPe-like identity upon increased activation of canonical Wnt signaling in hESC-derived organoids.

We sought to examine the effect of increased activation of canonical Wnt signaling in the hESC-derived organoids. We tested a range of concentrations of CHIR (3 μM to 12 μM) in the cocktail added to the organoids after 18 days *in vitro*, keeping the BMP4 concentration constant. The organoids were examined for TTR, AQP1, and OTX2 expression by immunohistochemistry, qPCR analysis, and RNA-seq (Figure 7). As early as 7 days post CHIR treatment (25 days *in vitro*), 3 μM-treated organoids displayed multiple domains of TTR decorating the perimeter, but 12 μM-treated organoids displayed no detectable expression of TTR (Figure 7C; Supplementary Figure 3C). We tested the dose-response to CHIR treatment by examining the expression of TTR, AQP1, and OTX2 in organoids using the different CHIR regimens. Whereas all three proteins appeared along the perimeter of 3 μM CHIR-treated

255 organoids, their expression was undetectable at all higher concentrations (Figure 7D;
256 Supplementary Figure 3D). qPCR analysis confirmed this finding: upon treatment with 3 µM
257 CHIR, *TTR, AQP1,* and *OTX2* displayed a significant increase in fold-expression over the baseline
258 (untreated 18-day organoids). However, treatment with 12 µM CHIR appeared to suppress the
259 expression of these genes to levels below the baseline (Figure 7E). In contrast, *LEF1* expression
260 correctly reflected the increased activation of canonical Wnt signaling by displaying a graded
261 increase in fold expression above baseline upon 3 µM and 12 µM CHIR treatment (Figure 7F).
262
263 To obtain a comprehensive picture of the effect of increased canonical Wnt pathway
264 activation on hESC-derived organoids, we performed RNA-seq of 3 µM and 12 µM CHIR-treated
265 samples. Several major CPe markers detected in the 3 µM-treated condition are suppressed
266 upon 12 µM CHIR treatment (Figure 7G). These include markers of differentiated CPe such as
267 *AQP1, TTR, OTX2*; genes that encode proteins that participate in forming tight junctions that are
268 typical of the CPe, such as *CLDN1, 2, 5,* and *TJP1,3*; and those that encode transporters or ion
269 channels such as *SLC4A10, CLIC6, SLC12A7, and SLC12A8.*
270
271 In summary, multiple lines of analysis confirm that the CPe-like differentiation seen in
272 hESC-derived organoids upon low activation of the canonical Wnt pathway is suppressed upon
273 increased activation of this pathway.

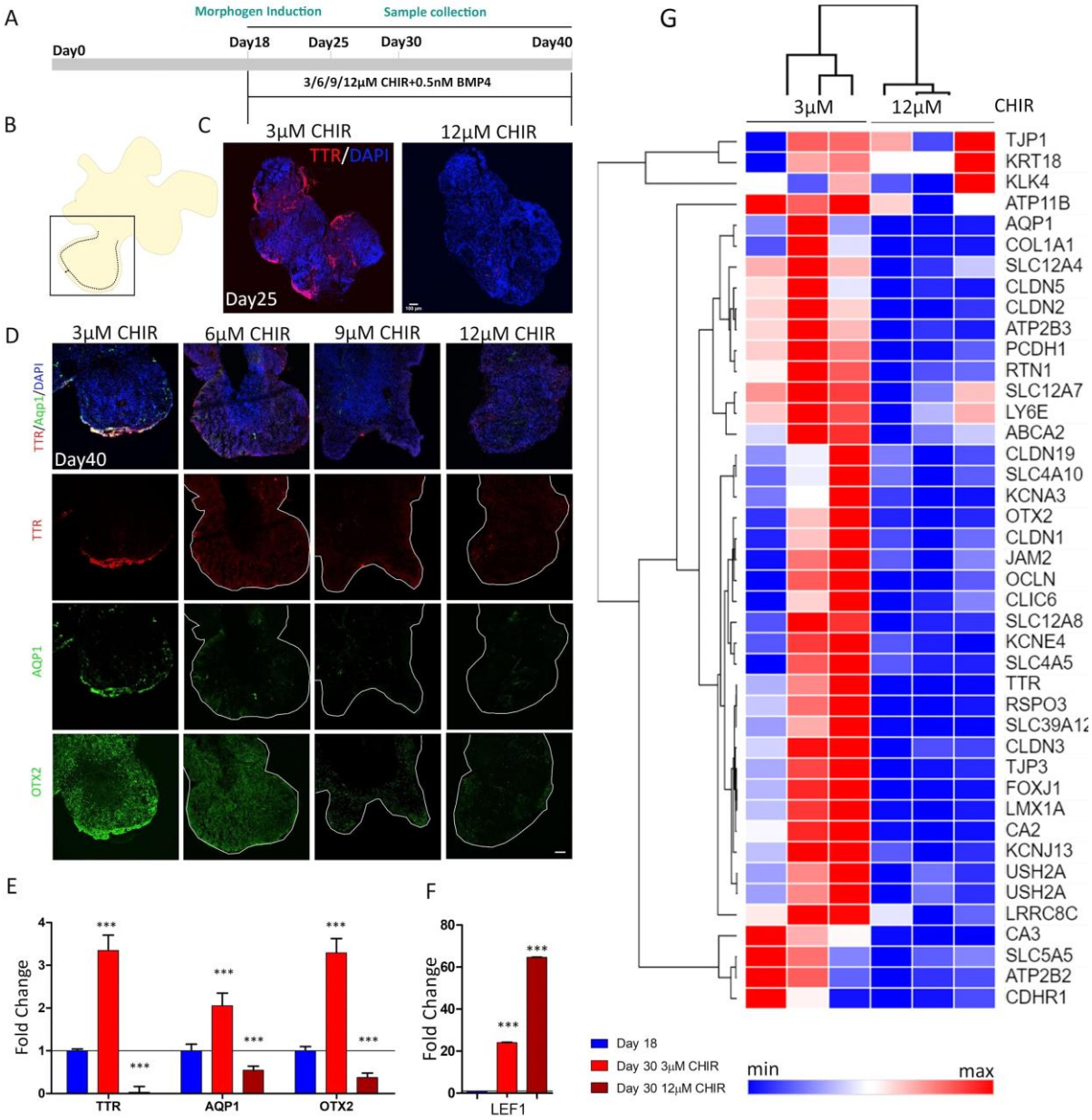

Figure 7. High activation of the canonical Wnt pathway in hESC-derived organoids causes suppression of CPe markers.

(A) Schematic presentation of the protocol for treatment of organoids with canonical Wnt agonist CHIR. (B, C) The CP marker TTR is expressed in the periphery of a day 25 organoid exposed to 3 μM, but not when exposed to 12 μM CHIR, from day 18. (D) High magnification images (boxed region shown in B) of serial sections of a day 40 organoid exposed to 3 μM reveal the expression of TTR, AQP1, and OTX2 in the periphery. This expression is reduced or undetectable upon exposure to higher concentrations of CHIR (6/ 9/12 μM). Additional examples are in Supplementary Figure 3.

(E) q-PCR analysis shows that the expression of the CP markers *TTR*, *AQP1*, and *OTX2* is upregulated in organoids at day 30 organoids exposed to 3 μM CHIR from day 18. This

increased expression is lost upon treatment with 12 μM CHIR for the same period. (F) *LEF1* expression displays a stepwise increase upon 3 μM and 18 μM CHIR treatment, consistent with increased activation of the canonical Wnt pathway. Group means were compared using one-way *ANOVA* followed by posthoc Tukey's multiple comparison test, * p-value<0.05, ** p-value<0.01, *** p-value<0.001(N=4). (G) Heatmap comparing normalized RNA-seq reads for 3 μM and 12 μM CHIR-treated organoids. Several CP-enriched genes are downregulated with increased activation (12 μM CHIR) of canonical Wnt signaling. All scale bars are 100 μm.

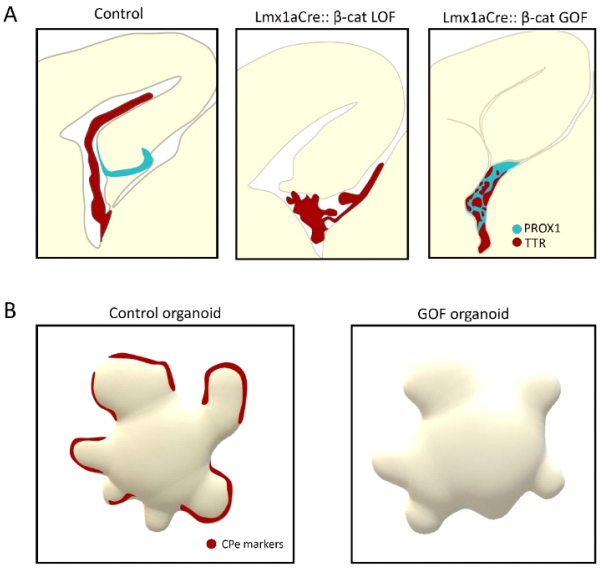

Figure 8: Summary

(A) Schematic presentation showing that decreased Wnt signaling in the CPe leads to a dysmorphic appearance of the choroid plexus while an increase in Wnt signaling transforms the CPe into PROX1 positive DG granule cell-like identity. (B) hESC derived CP organoids lose their choroid identity upon an increase in Wnt signaling following treatment with high CHIR concentration.

302 ## Discussion

303

304 We report that β-CATENIN, which mediates canonical Wnt signaling, is required for the
305 normal development of the telencephalic CP. Furthermore, hyper-activation of canonical Wnt
306 signaling resulting from constitutive activation of β-CATENIN alters gene expression and
307 disrupts CPe fate both in the mouse embryo and in hESC-derived CP organoids. Therefore, a
308 finely regulated balance of canonical Wnt signaling appears to be critical for CPe differentiation
309 in the mammalian brain.

310 As one of the major signaling pathways that regulate multiple aspects of cellular, tissue,
311 and organ development and function, canonical Wnt signaling is tightly controlled, and
312 perturbations of this pathway cause an array of defects: In human hair follicle morphogenesis,
313 loss or constitutive activation of β-CATENIN levels leads to tumor formation or defective
314 differentiation, respectively (Huelsken et al., 2001, Kajino et al 2001). In several cases,
315 constitutive activation of β-CATENIN appears to transform the identity of the cells in which this
316 perturbation is introduced: the mouse epiblast prematurely displays epithelial to mesenchymal
317 transition (Kemler et al., 2004); endothelial cells of the midbrain transform to a "barrier cell"
318 identity (Wang et al., 2019), and airway epithelial cells take on a neuroendocrine-like fate (Li et
319 al., 2009). Our report of a transformation of CP epithelial cells to a neuronal fate upon
320 constitutive activation of β-CATENIN has parallels with what has been seen in other systems.

321 An unexpected feature of the CPe-to-neuronal transformation, however, is that the
322 transcriptomic profile of the β-catenin GOF CP is hippocampal-like, not CR cell-like. It has been
323 well established that the hem is the progenitor domain for both CPe and CR cells (Louvi et al.,
324 2007). This fate choice is regulated by transcription repressors of bHLH family members HES1,
325 2, and 3, which promote epithelial identity by suppressing neurogenic genes and inducing BMP
326 signaling. Upon loss of all three *Hes* genes, the hem upregulates the pro-neuronal factor
327 *Neurog2* and produces CR cells instead of CPe cells (Imayoshi *et al.*, 2008). How might
328 hippocampal-like cells arise from this lineage? A study using Lmx1aCre-driven lineage analysis
329 reported that in addition to CR and CPe cells, a small population of hippocampal cells also
330 appears to originate in the hem, regulated by LMX1a itself (Chizhikov et al., 2010). Taking into
331 consideration that canonical Wnt signaling is known to be both necessary and sufficient for
332 hippocampal fate specification (Lee et al., 2000; Machon et al., 2007; Solberg et al., 2008), β-
333 catenin GOF may drive the hem/CPe to this third "hippocampal" branch of the hem lineage.
334 Together, the results suggest that the two neuronal derivatives of the hem may be regulated by
335 distinct mechanisms, and this motivates a careful analysis of how different regulatory pathways
336 may interact to drive differentiation along the non-neuronal and neuronal lineages arising from
337 the hem.

338 Activation of the canonical Wnt pathway is often tumorigenic (Kim and Jeong 2019).
339 Human cases of CP carcinoma are associated with mutations in exon 3 of the *ß-CATENIN* gene
340 that lead to its constitutive activation (Kim & Jeong, 2019). Mouse models of CP papilloma that
341 are generated by constitutive activation of NOTCH signaling show concomitant upregulation of
342 the canonical Wnt pathway (L. Li et al., 2016). It is not clear what mechanisms control whether
343 canonical Wnt activation causes cell fate transformations or tumorigenic changes, but it is likely
344 that a crosstalk with other major signaling pathways is involved. The β-catenin GOF mouse CP
345 offers a useful and accessible model in which this question can be examined.
346
347 The hem also expresses the non-canonical WNT5A, which is required for normal CPe
348 cytoarchitecture, apicobasal polarity, and overall size and complexity of the CP (Langford et al.,
349 2000). Together with the established role for BMPs in the specification of the CP (Hebert *et al.*,
350 2002; Watanabe *et al.*, 2012), it is apparent that the known signaling molecule families
351 expressed in the hem, the BMPs, canonical and non-canonical WNTs, are each critical for CP
352 development. Our findings regarding the role of the canonical Wnt pathway motivate a careful
353 examination of how these pathways crosstalk with each other to execute the specification,
354 cytoarchitecture, morphogenesis, and expansion of the non-neuronal choroid plexus arising
355 from neuroepithelium.
356
357 Key features of β-catenin GOF in the CP include dysregulation of factors that are
358 essential for the CP to produce the CSF. These include several anion cation exchangers, ion
359 channels, and solute transporters each of which acts as regulators of CSF composition: a
360 sodium-potassium ATPase, *Atp1a1* (Ernst et al., 1986); an epithelial sodium channel, *Scnn1a*
361 (Amin et al., 2009); an inward rectifying potassium channel, *Kcnj13* (Cornejo et al., 2018); a
362 voltage-gated potassium channel, *Kcna1* (Speake et al., 2003); and a sodium-potassium-chloride
363 cotransporter 1, *Nkcc1*, that modulates water transport underlying CSF production (Steffensen
364 et al., 2018) and is also associated with Blood CSF barrier disruption (Kim & Jung., 2012).
365 Furthermore, the expression of several genes encoding transporters for glucose, chloride, and
366 amino acids, is also downregulated in the β-catenin GOF CP. Together, the data indicate that
367 canonical Wnt signaling is critical to enabling the CPe to produce normal CSF. Mutations in exon
368 3 of *ß-CATENIN* in humans result in stabilization of β-CATENIN (Bjorklund et al., 2008), similar to
369 that seen in the β-catenin GOF mouse model (Harada et al., 1999). Human studies have focused
370 on the association of these mutations with carcinomas (Gao and Zang., 2018; Kim & Jeong.,
371 2019), but no associated effects on the CSF have been explored. Our study identifies a major
372 developmental outcome of the β-catenin GOF perturbation in terms of its effect on the
373 composition of the CSF.
374
375 The formation of CPe in hESC-derived organoids requires low activation of the canonical

376 Wnt pathway together with BMP signaling. Loss of CPe fate in these organoids upon high
377 activation of the canonical Wnt pathway indicates conservation of the role of this pathway in
378 the development of the CPe. hESC-derived organoids are not only an excellent system to study
379 conserved developmental mechanisms but also offer the opportunity to test for subtle effects
380 of altered CP/CSF status on neuronal cells. Depending on the protocol used, the organoids
381 develop into fluid-filled cysts that contain several human CSF proteins (Pellegrini et al., 2020).
382 These organoids are permeable to small molecules and are excellent model systems to test
383 modalities of drug delivery to the CNS (Pellegrini et al., 2020). Thus, hESC-derived CP organoids
384 offer a suitable system to model both diseases as well as modalities for treatment.
385
386 In conclusion, we demonstrate that the developing choroid plexus expresses
387 components of the canonical Wnt signaling pathway in embryonic mouse and human brains.
388 Both loss and gain of function of β-CATENIN disrupt CPe development, indicating that this
389 pathway is likely to be under a finely tuned regulation *in vivo*. These findings motivate future
390 studies on how this regulation is achieved and may provide a mechanistic basis for subtle
391 deficits in CP/CSF function connected to the disruptions of the canonical Wnt pathway function
392 in this system.

Supplementary Figures

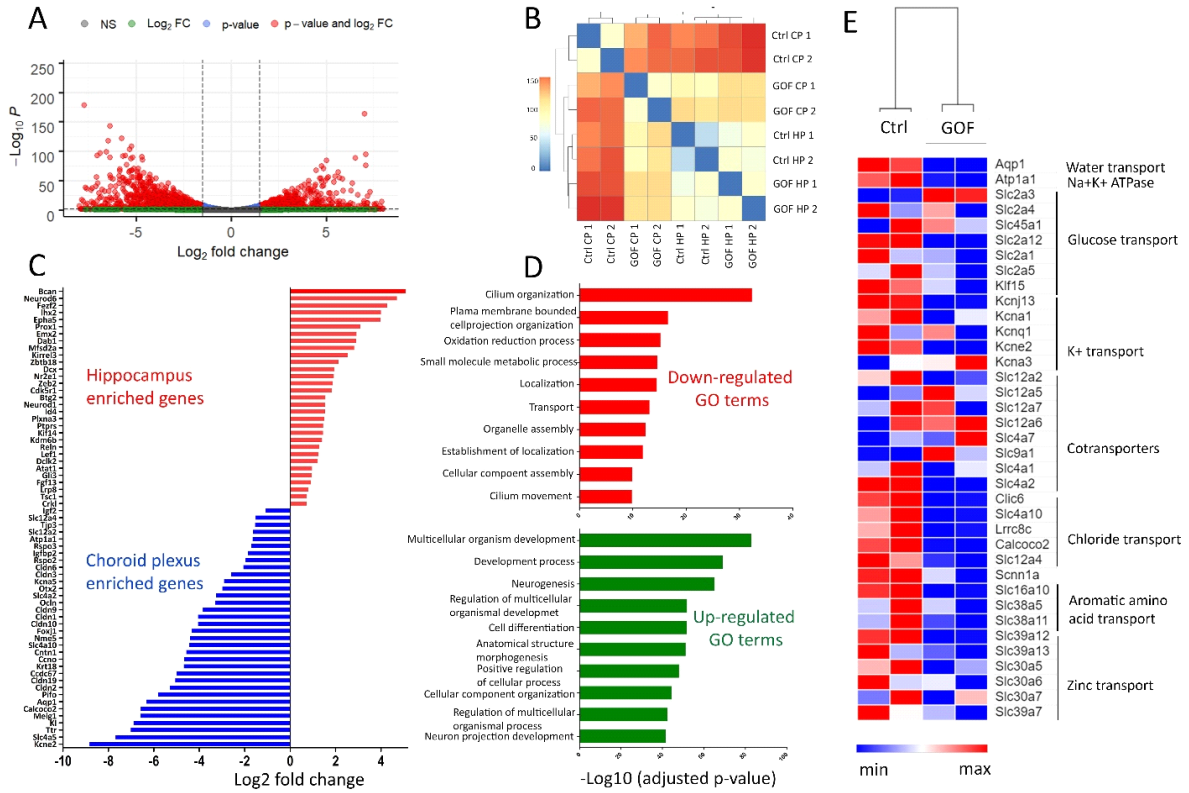

Supplementary Figure 1: Analysis of differentially expressed gene sets in the control and β-catenin GOF CP and Hippocampus.

(A-E) Analysis of RNA-seq data from the control (Ctrl) versus Lmx1aCre:: β-catenin GOF CP and Hippocampus (HP). (A) Volcano plot showing Differentially Expressed Genes in the control and β-catenin GOF CP (B) Sample correlation matrix revealing the similarity of the β-catenin GOF CP to wild type HP rather than the wild type CP. (C) DEG reveals the loss of CP enriched genes and the gain of HP genes in the GOF CP. (D) GO analysis of upregulated and downregulated genes from (A). (E) Heatmap of normalized read counts of genes belonging to different classes of transporters expressed in wild type and the β-catenin GOF CP.

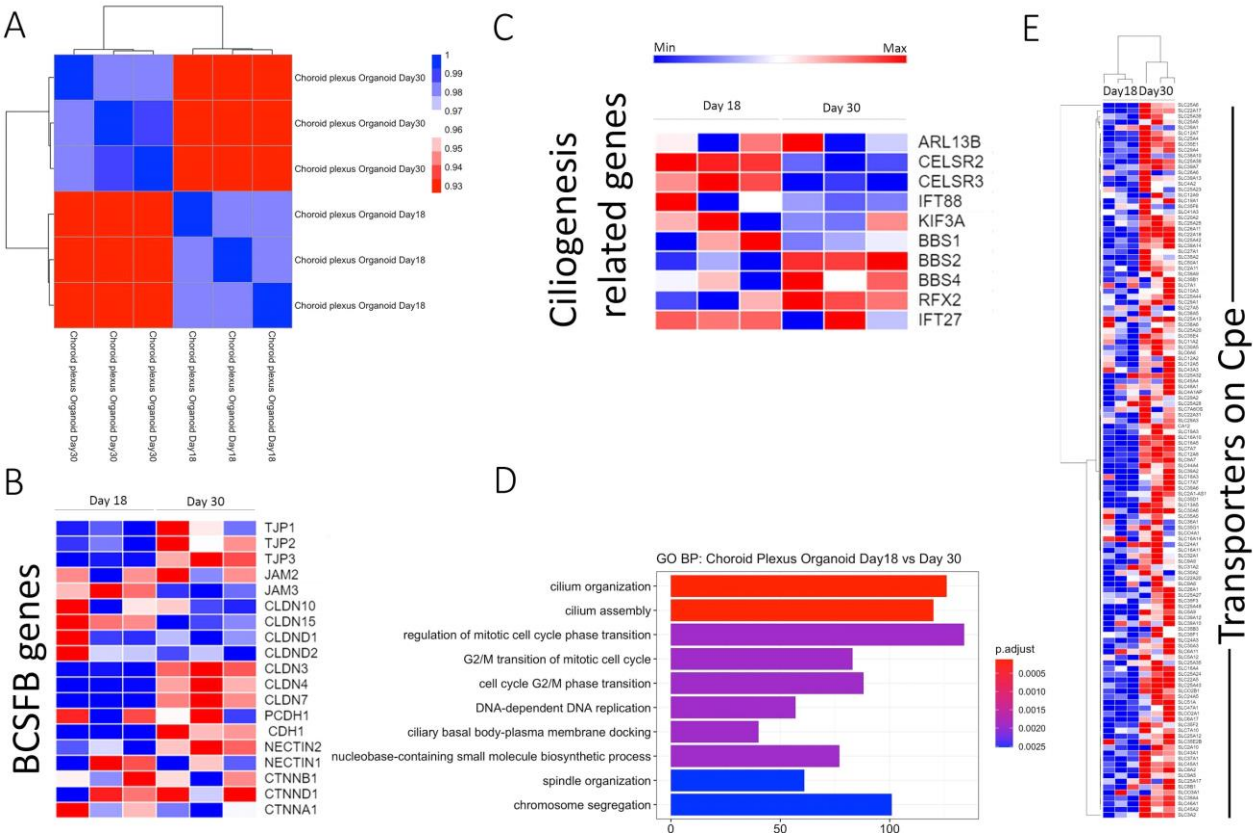

Supplementary Figure 2: Characterization of CPe-like differentiation in hESC organoids

(A-E) A comparison of transcriptomics data from day 18 and day 30 organoids. (A) Sample correlation matrix (B, C). Heat map of the normalized reads reveals that several BCSF genes are upregulated (B) and ciliogenesis-related genes are differentially regulated (C). (D) GO analysis (E) Heat map plotted from normalized reads shows an overall upregulation of transporter genes (belonging to the Slc gene family) in day 30 organoids.

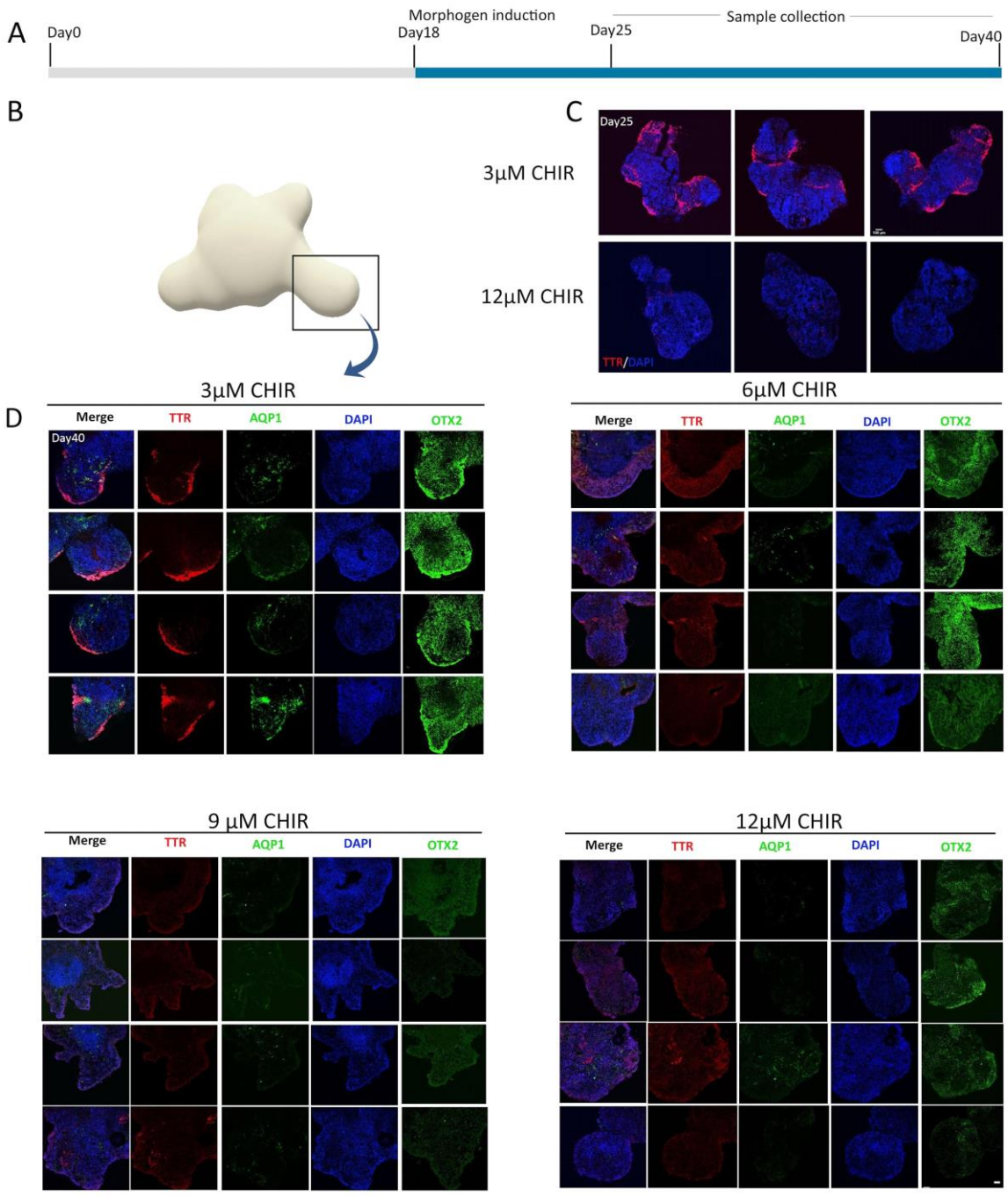

Supplementary Figure 3: High activation of the canonical Wnt pathway in hESC-derived organoids causes suppression of CPe markers.

Additional examples of data shown in Figure 7 C and D. (A) Scheme showing the protocol for treatment with canonical Wnt agonist CHIR (C) CP marker TTR is expressed in the periphery of day 25 organoids (n=3) exposed to 3 μM, but not 12 μM CHIR, from day 18. (D) High magnification images (boxed region shown in B) of serial sections of four examples of day 40 organoids exposed to 3 μM reveal the expression of TTR, AQP1, and OTX2 in the

421 periphery. This expression progressively decreases and is undetectable upon increasing
422 exposure to higher concentrations of CHIR (6/ 9/ 12 µM). All scale bars are 100 µm.
423

424 Material and methods

425

426 **Tissue collection:**

427 Mice: All animal protocols were approved by the Institutional Animal Ethics Committee of the
428 Tata Institute of Fundamental Research, Mumbai, India. The mouse lines used in this study
429 were kind gifts from Kathy Millen (Center for Integrative Brain Research, Seattle Children's
430 Research Institute; Lmx1aCre line, Chizikov and Millen., 2004), Raj Awatramani (Department of
431 Neurology and Center for Genetic Medicine, Northwestern University Feinberg Medical School
432 Chicago, Illinois; β-catenin LOF mice, Joksimovic and Awatramani., 2014). The Ai9 mouse line
433 was obtained from JAX labs Stock No. 007909. Noon of the day of the vaginal plug was
434 designated as embryonic day 0.5 (E0.5). Control embryos were littermates that did not carry
435 the Lmx1aCre allele. Since the Lmx1aCre transgene is on the X-Chromosome and females
436 showed mosaic expression of the transgene due to random X inactivation, only male
437 embryos/pups with the Lmx1aCre were used for analysis. A total of 34 wild-type (Figures 1-4), 9
438 β-catenin LOF (Figure 2), and 15 β-catenin GOF (Figure 3, and 4) embryos/pups were used for in
439 situ hybridisation and immunohistochemistry analysis. Breeding colonies were maintained with
440 the female breeders carrying the Lmx1aCre transgene since this Cre line shows germline
441 recombination in the testis. The sex of the embryos was determined by examining the gonads
442 from E12.5 onwards.
443 Primers used were: Cre F: ATTTGCCTGCATTACCGGTC, Cre R: ATCAACGTTTTCTTTTCGG, Cre
444 positive DNA shows a band at 350bp. Other mouse lines were genotyped using references
445 mentioned before.
446

447 Human: Fetal brain specimens were obtained from either medically indicated or spontaneous
448 abortions. The Institutional Ethical Review Board of the School of Medicine, University of
449 Zagreb and University Hospital Center Zagreb has approved the procedure for the collection of
450 postmortem brain samples (UHC Zagreb EP02/21AG; UZSM: 641-01/19-02/01). The fetal age
451 was estimated based on crown-rump length (CRL, in mm), pregnancy records, and histological
452 findings, and expressed as GW. In addition, the correlation of maturational parameters (CRL,
453 body mass, pregnancy records, and sonographic examination) revealed no evidence of growth
454 retardation or malformations. Finally, specimens in which subsequent postmortem analysis
455 revealed macroscopically or microscopically identified pathological changes, or postmortem
456 autolytic changes, were excluded.
457
458

459

460 **Immunohistochemistry**

461 Mouse sections and organoids: Mouse brain sections /organoid sections were mounted on plus
462 slides (Catalogue number: EMS 71869-11) and dried for 2-3 hours. Slides were transferred to a
463 slide mailer (Catalogue number: EMS 71549-08) containing PBS+0.01% TritonX-100 for 10
464 minutes followed by a wash with PBS+0.03% TritonX-100 for 5 minutes. For antigen retrieval,
465 sections were boiled in a 10mM sodium citrate buffer (pH=6) at 90^0C for 10 minutes using a
466 water bath. Slides were cooled to room temperature and washed with PBS+0.01% TritonX-
467 100 for 10 minutes. Blocking (5% horse serum /Lamb serum in PBS + 0.1% TritonX-100) for 1
468 hour followed by overnight primary antibody incubation at 4°C. Secondary antibody
469 incubation was performed at room temperature for 2 hours followed by 3 washes with 1x PBS.
470 Slides were mounted using vector shield mounting media (Vector laboratories H-1000-10) and
471 imaged in an Olympus FluoView 1200 confocal microscope. The primary antibodies used were:
472 LEF1 (rabbit,1:200 CST catalogue # C12A5), β-CATENIN (mouse 1:200,BDbiosciences catalogue #
473 610153),RFP(rabbit,1:200 Abcam catalogue # ab62341)FZD1 (rabbit,1:100 catalogue #
474 LS-A4150),AXIN2 (rabbit ,1:200 Abcam catalogue # ab185821),TTR (rabbit 1:100 ,DAKO
475 catalogue # A0002), AQP1 (mouse 1:200 SCBT catalogue # sc25287),OTX2(mouse,1:200SCBT
476 catalogue # sc-514195),OTX2(1:500,invitrogen,PA5-39887),AQP1 (rabbit, 1:200,invitrogen
477 catalogue # MA5-32593),E-CADHERIN(mouse,1:200,SCBTcatalogue#sc21791). Secondary
478 antibodies used were following: Goat Anti Rabbit Alexa fluor 488 (1:200, Invitrogen catalogue #
479 A11034), Goat Anti mouse Alexa fluor 594 (1:200, Invitrogen catalogue # R37121), Goat Anti
480 Rabbit Alexa fluor 568 (1:200, Invitrogen catalogue # A11011), Donkey Anti goat Alexa fluor 568
481 (1:200, Invitrogen catalogue # A32814).

482 Human: The entire brains were fixed by immersion in 4% paraformaldehyde in 0.1 M phosphate
483 buffer saline (pH=7.4). Subsequently, tissue blocks were embedded in paraffin wax. Serial
484 sections were cut (5 µm) and stained. The cresyl violet staining was used to delineate
485 cytoarchitectonic boundaries, while adjacent sections were labelled using immunofluorescence
486 with various antibodies. The following primary antibodies were used: (1) rabbit polyclonal anti-
487 Axin 2, (ab185821, Abcam, Cambridge, United Kingdom); (2) the rabbit polyclonal Frizzled 1
488 antibody, FZD1 (LS-A4150, LSBio, Seattle, Washington, SAD); (3) the monoclonal rabbit LEF1
489 antibody (C12A5, Cell Signaling, Leiden, Netherlands); (4) the mouse monoclonal aquaporin1
490 antibody, AQP1 (sc-25287, Santa Cruz, Dallas, Texas, SAD); (5) the rabbit non-phospho (Active)
491 βCatenin (D13A1, Cell Signaling, Leiden, Netherlands); (6) the monoclonal mouse OTX2
492 antibody (MA5-15854, Invitrogen, Carlsbad, California, SAD); (7) the mouse monoclonal Beta-
493 Catenin, (M3539, Dako Agilent, Santa Clara, California, SAD).

494 The dewaxing of sections was performed in xylol for 5 min, and a series of alcohol solutions
495 (100%, 96% 70%) for 2 min. Slides were then washed in PBS with 0.03% triton (10min).

496 The antigen retrieval was performed in citrate buffer pH6.0 and microwave (800W) for 10
497 minutes. The slides were cooled at room temperature and immersed in a blocking solution (PBS
498 containing 3 % bovine serum albumin, BSA, and 0.01 % Triton X-100, all from Sigma, St. Louis,
499 MO) for 30 min. to prevent nonspecific background staining. Sections were then incubated with
500 primary antibodies for 48 h at 4˚C (AXIN2 1:100, FZD1 1:100, LEF1 1:100, AQP1 1:100, OTX2
501 1:50, β-Catenin cell signaling 1:400, β-Catenin Dako 1:200), washed and subsequently incubated
502 with secondary anti-mouse or anti-rabbit antibodies diluted in PBS (at 1:1000) for 2 h at the
503 room temperature. For visualization of the specific immune reactivity following secondary
504 antibodies were used according to the laboratory protocol (Culjat and Jovanov-Milosevic,
505 2019): the donkey anti-mouse IgG Alexa fluor-plus 488, donkey anti-rabbit IgG Alexa fluor-
506 plus 647, donkey anti-rabbit IgG 488, donkey anti-mouse IgG Alexa-fluor 546 were used.
507 Sections were covered with a mounting medium containing DAPI. Negative controls were
508 included in all experiments by replacing the primary antibody with a blocking solution. No
509 immunolabeling was detected in control sections.

510 **In situ hybridization**

511 Mouse brains were sectioned using a freezing microtome (Leica SM2000R Sliding Microtome)
512 to a thickness of 20 µM. Sections were mounted on super frost plus slides (Catalogue #: EMS
513 71869-11), fixed with 4% (w/v) paraformaldehyde for 15 minutes, washed three times with PBS.
514 The sections were then treated with proteinase K dissolved in Tris-EDTA buffer (1 µg/ml). Post
515 fixation was performed in 4% PFA for 15 minutes and the sections were washed three times in
516 PBS. Hybridization was performed for 16 h at 70°C in a buffer containing 50% (v/v) formamide,
517 2X SSC, and 1% (w/v) SDS. Digoxigenin (DIG)-labelled cRNA probes were used for hybridization
518 and were prepared from respective plasmids using in-vitro transcription. After hybridization,
519 three stringent washes (for 45 minutes each) were performed in solution X (50% formamide, 2X
520 SSC, and 1% SDS) followed by a wash with 2XSSC and then 0.2XSSC. Blocking was performed
521 for 1 hr with 10% horse serum in TBST (Tris-buffered saline pH 7.5 with 0.1% Tween-20).
522 Sections were incubated in alkaline phosphatase-conjugated anti-DIG (Digoxygenin) antibody
523 Fab fragments (1:5000; Roche, catalogue #12486523) at 1:5000 in the blocking buffer and
524 incubated at 4°C overnight. The color reaction was performed using NBT/BCIP substrate
525 (Roche, 4-nitroblue tetrazolium chloride, catalogue #70210625; 5-Bromo- 4-chloro-3-indolyl
526 phosphate, catalogue #70251721). Counterstaining was performed using Fast Red (Sigma-
527 Aldrich, catalogue # N3020). Slides were dried and coverslipped using DPX mounting reagent
528 (SDFCL, catalogue #46029).

529

530

531 **Image acquisition and analysis**

532 Bright field images were acquired using Zeiss Axioskop-2 plus microscope equipped with a
533 Nikon DS-fi2 camera and associated software. Mouse sections were imaged in Olympus
534 FluoView 1200 confocal microscope and the human brain sections were imaged in Olympus
535 FluoView 3000 confocal microscope. All the organoid sections were imaged using the Andor
536 Dragonfly spinning disk confocal microscope system. All the image analysis was done on Fiji-
537 ImageJ and/or Adobe Photoshop CS6.

538 **Generation of hESC derived organoids**

539 The human ES cell line WIBR3, obtained from the Whitehead Institute for Biomedical Research,
540 (https://hpscreg.eu/cell-line/WIBRe001-A), was used in compliance with all applicable statutes
541 and regulations and compliance with applicable guidelines (including the NAS Guidelines or
542 guidelines of the International Society for Stem Cell Research as relevant to the conduct of
543 human embryonic stem cell research ["ISSCR Guidelines"]. The line was cultured on a MEF
544 (mouse embryonic fibroblast) feeder layer. To maintain the pluripotent state, a customized
545 human Naïve media with 40 µM Rock Inhibitor Y-27632 was used as described in Karzbrun et al
546 2018. Differentiation of hES aggregates into Choroid plexus like organoid was done using a
547 protocol described in Sakaguchi et al 2015 (Sakaguchi et al., 2015). Briefly, hESC colonies were
548 grown in a Matrigel plate till confluency, then the cells were dissociated with trypsin and rapidly
549 reaggregated in an ultra-low attachment 96 well V bottom plate (9000 cells per well) containing
550 a media termed as SA1 media. This media contains DMEM (Invitrogen cat # 11965092)
551 supplemented with 20% (vol/vol) KSR (Invitrogen cat # 10828028), 0.1mM non-essential amino
552 acids (Invitrogen cat # 11140050), 1mM pyruvate (Invitrogen cat # 11360070), 0.1mM 2-
553 mercaptoethanol (Invitrogen cat # 21985023), 100U/ml penicillin and 100 mg/ml streptomycin.
554 0.3 mM IWR1e (tankyrase inhibitor, MedChemExpress cat# HY-12238) and 5 mM SB431542
555 (TGFβ inhibitor; MedChemExpress HY-10431) were added to culture from day 0 to day 18 (day
556 of aggregation was defined as day 0). The culture media used after day 18 till day 40 was
557 termed as SA2, which contains DMEM/F-12 (Invitrogen cat # 21331020), GlutaMAX(TM) (Gibco)
558 supplemented with 1% N-2 supplement (Invitrogen cat # 17502048), 1% Chemically Defined
559 Lipid Concentrate (Invitrogen cat # 11905031), fetal bovine serum (FBS; 10% vol/vol), 3 µM
560 CHIR 99021 (GSK3 inhibitor; MedChemExpress cat # HY-10182) and 0.5 nM BMP4 (R&D cat #
561 314-BP-050) under normoxia condition. The medium was changed once every 2 days. From day
562 5 onwards the plates were kept on an orbital shaker placed inside the incubator. On day 18
563 the organoids were transferred from 96 well plates to 10 cm ultra-low attachment plate (6
564 organoids per plate) and kept on an orbital shaker inside the incubator. For sample collection,
565 the organoids were rinsed with 1x PBS for 2 times, then either flash-frozen for RNA-seq
566 experiments or transferred to a small dish containing 4% PFA solution for

567 immunohistochemistry. A total of 12 control organoids (3 µM CHIR) were used for Figure 6. For
568 Figure 7, 14 organoids (3 µM CHIR), 9 organoids (6 µM CHIR), 5 organoids (9 µM CHIR treated),
569 and 14 organoids (12 µM CHIR treated), were used immunohistochemistry analysis.

570 **RNA sequencing, library preparation, and analysis of mouse tissues**

571

572 The mouse CP was dissected from E14.5 control and β-catenin GOF brains and stored in Trizol®
573 reagent. Extracted RNA of 1 µg (RIN > 7.5, measured using the Agilent 2100 bio analyzer) from
574 CPe dissected from 4 embryos was pooled for each of two biological replicates. After library
575 preparation, sequencing was performed on the Illumina platform to achieve 100bp or 150bp
576 reads to generate 30 Million paired-end reads per sample. FastQ QC was performed as
577 described in (Andrews, S 2010), and reads > 30 Phred scores were aligned using HISAT2 (D.Kim
578 et al., 2019). Feature counts were used to quantify the number of reads per transcript.
579 Differential expression analysis was performed using DESeq2 (Love et al., 2014) on the R
580 platform (v3.6.3). Genes showing |log2 Fold change|≥1 were used for further analysis. Gene
581 ontology analysis was performed using geneontology.org or gprofiler.org. Semantics were
582 summarized using "REVIGO" (Supek et al., 2011), and bar plots were created with GraphPad
583 Prism V7.0 for Windows, GraphPad Software, San Diego California USA, www.graphpad.com).
584 Heat maps and sample correlation plots were plotted using R studio. Gene-based heatmaps
585 were plotted using normalized reads on Morpheus (Morpheus,
586 https://software.broadinstitute.org/morpheus)

587

588 **RNA sequencing, library preparation, and analysis of organoids**

589

590 Organoids generated in figure 6 and supplementary figure 2, were pooled such that for one
591 biological replicate 3 organoids were used and three such biological replicates were performed
592 for day 18 and day 30 organoids. Bulk MARS-seq libraries were produced from 50ng of total
593 RNA as previously described (Meador et al.,2014). Libraries were then sequenced with 75bp
594 single-end read on Illumina Nextseq500 platform and FASTQ files were processed and analyzed
595 using UTAP (Kohen et al., 2019). Briefly, sequenced reads were trimmed using cutadapt
596 (parameters: -a adaptor -a "A {10}" –times 2 -u 3 -u -3 -q 20 -m 25) (M Martin., 2011) and were
597 mapped to hg38 indexed reference genome using STAR (Dobin et al., 2013) v2.4.2a with the
598 following parameters: –alignEndsType EndToEnd, –out Filter Mismatch Nover Lmax 0.05, –two
599 pass Mode Basic). UMIs were counted after marking duplicates using HTSeq-count (Anders et
600 al., 2015) in union mode. For the number of reads per gene, 1000bp of 3' end Gencode
601 annotated transcripts were counted. The total RNA-seq from 3 µM and 12 µM CHIR treated
602 organoids (Figure 7) were done using TruSeq stranded mRNA library kit and sequenced by DNA
603 Link Sequencing Lab, Korea, on NovaSeq 6000, 100PE. Data were analyzed with the UTAP

604 pipeline (Kohen et al., 2019), where adapter trimming and reference genome alignment was
605 performed as described above. Read count per gene was done with STAR. Normalization of the
606 counts and differential expression analysis was performed using DESeq2 (Love et al., 2014) with
607 the parameters: betaPrior=True, cooks Cutoff=FALSE, independentFiltering=FALSE. Raw P
608 values were adjusted for multiple testing using the procedure of Benjamini and Hochberg.
609 Genes with log2FC >1 or <-1, p adjust < 0.05 and baseMean > 10 were considered as
610 differentially expressed. GO Biological process overrepresentation test on differentially
611 expressed genes between different time points of organoid growth was performed with the
612 package clusterProfiler (Yu et al., 2012).
613
614 **qPCR Analysis of organoids**
615
616 Total RNA of Day 18 and Day 30 organoids was extracted using the RNeasy Mini kit (Qiagen,
617 Germany) following the manufacturer's protocol and followed by DNAseI treatment. RNA
618 concentration was measured using Nanodrop (Thermo Scientific, MA, USA). cDNA was
619 synthesized using M-MLV reverse transcriptase (M3682, Promega, Wisconsin, USA). Real-Time
620 reactions were performed in triplicates using KAPA SYBR FAST qPCR Kit (2X) on QuantStudio 5
621 Real-time PCR system (Bio-Rad, CA, USA) following the manufacturer's recommendation.
622 Expression levels were normalized against GAPDH using the ΔΔ threshold cycle (Ct) method.
623 The fold changes were represented as mean±SEM. Primers: *AQP1* Fw: 5'-
624 TGGACACCTCCTGGCTATTG-3' Rw: 5'-GGGCCAGGATGAAGTCGTAG-3', *LEF1* Fw: 5'-
625 AGAACACCCCGATGACGGA-3' Rw: 5'-GAGGGTCCCTTGTTGTAGAGG-3', *TTR* Fw: 5'
626 ATCCAAGTGTCCTCTGATGGT 3' Rw: 5' GCCAAGTGCCTTCCAGTAAGA 3', *OTX2* Fw: 5'-
627 AGAGGACGACGTTCACTCG-3' Rw: 5'-TCGGGCAAGTTGATTTTCAGT-3'.
628
629 **Data availability:** The RNA-seq data described in the manuscript are deposited in the GEO
630 database (Accession number: GSE162784 and GSE162808). All other codes are available on
631 request with the corresponding authors.

632 ## Acknowledgments

633 We thank K. Millen (Seattle Children's hospital) for the kind gift of the Lmx1aCre mouse line;
634 Shital Suryavanshi and the animal house staff of the Tata Institute for Fundamental Research
635 (TIFR) for excellent support. This work was supported by a Wellcome Trust-Department of
636 Biotechnology India Alliance Early Career Fellowship (IA-E-12-1-500765; MC); by the Canada-
637 Israel Health Research Initiative, jointly funded by the Canadian Institutes of Health Research,
638 the Israel Science Foundation, the International Development Research Centre, Canada and the
639 Azrieli Foundation (ST); intramural funds from TIFR-DAE (12-R&D-TFR-5.10-0100RTI2001).

640 Research in the Reiner lab is supported by ISF-National Science Foundation of China (NSFC) joint

research program (Grant No. 2449/16), with the aid of a grant no. 2397/18 from the Canadian Institutes of Health Research (CIHR), the International Development Research Center (IDRC), the ISF, a grant from the Ministry of Science & Technology, Israel & The Ministry of Science and Technology of the People's Republic of China., German-Israeli Foundation (GIF; Grant no. I-1476-203.13/2018), and United States-Israel Binational Science Foundation (BSF; Grant No. 2017006). In addition, by the Helen and Martin Kimmel Institute for Stem Cell Research, Nella and Leon Benoziyo Center for Neurological Diseases, David and Fela Shapell Family Center for Genetic Disorders Research, Brenden-Mann Women's Innovation Impact Fund, Richard F. Goodman Yale/Weizmann Exchange Program, The Irving B. Harris Fund for New Directions in Brain Research, Irving Bieber, M.D. and Toby Bieber, M.D. Memorial Research Fund, Leff Family, Barbara & Roberto Kaminitz, Sergio & Sônia Lozinsky, Debbie Koren. Jack and Lenore Lowenthal, Dears Foundation. O. R. is incumbent of the Berstein-Mason professorial chair of Neurochemistry and Head of M. Judith Ruth Institute for Preclinical Brain Research.

The study on the human brains was financed by Croatian Science Foundation projects IP-2019-04-3182; DOK-2018-01-3771; DOK-2015-10-3939 to NJM and the Scientific Centre of Excellence for Basic, Clinical, and Translational Neuroscience (GA KK01.1.1.01.0007 funded by the European Union through the European Regional Development Fund). The collaboration was initiated throughout COST Action 16118.

We thank the members of Tole lab, Reiner lab, and Jovanov lab for their valuable inputs and discussion.

661 ## References

662

663 Abu-Khaklil, A., Fu, L., Grove, E. A., Zecevic, N. & Geschwind, D. H. Wnt genes define distinct
664 boundaries in the developing human brain: Implications for human forebrain patterning. *J.*
665 *Comp. Neurol.* **474**, 276–288 (2004).

666 Amin, M. S., Reza, E., Wang, H., & Leenen, F. H. H. (2009). Sodium transport in the choroid
667 plexus and salt-sensitive hypertension. *Hypertension*, *54*(4), 860–867.
668 https://doi.org/10.1161/HYPERTENSIONAHA.108.125807

669 Anders, S., Pyl, P. T., & Huber, W. (2015). HTSeq-A Python framework to work with high-
670 throughput sequencing data. *Bioinformatics*, *31*(2), 166–169.
671 https://doi.org/10.1093/bioinformatics/btu638

672 Andrews, S. (2010). **FastQC**: A Quality Control Tool for High Throughput Sequence Data
673 http://www.bioinformatics.babraham.ac.uk/projects/fastqc

674 Björklund, P., Lindberg, D., Åkerström, G., & Westin, G. (2008). Stabilizing mutation of
675 CTNNB1/beta-catenin and protein accumulation analyzed in a large series of parathyroid
676 tumors of Swedish patients. *Molecular Cancer*, *7*, 1–8. https://doi.org/10.1186/1476-4598-7-53

677 Brault, V., Moore, R., Kutsch, S., Ishibashi, M., Rowitch, D. H., McMahon, A. P.,
678 Sommer, L., Boussadia, O., & Kemler, R. (2001). Inactivation of the β-catenin gene by Wnt1-Cre-
679 mediated deletion results in dramatic brain malformation and failure of craniofacial
680 development. *Development*, *128*(8), 1253–1264.

681 Castañeyra-Ruiz, L., González-Marrero, I., Hernández-Abad, L. G., Carmona-Calero, E. M.,
682 Meyer, G., & Castañeyra-Perdomo, A. (2016). A Distal to Proximal Gradient of Human Choroid
683 Plexus Development, with Antagonistic Expression of Glut1 and AQP1 in Mature Cells vs.
684 Calbindin and PCNA in Proliferative Cells. *Frontiers in Neuroanatomy*.
685 https://doi.org/10.3389/fnana.2016.00087

686 Chip, H. B. B., Park, T., Mustafaoglu, N., Herland, A., Hasselkus, R., Mannix, R., Fitzgerald, E. A.,
687 Prantil-baun, R., Watters, A., Henry, O., Benz, M., Sanchez, H., Mccrea, H. J., Goumnerova, L. C.,
688 Song, H. W., Palecek, S. P., Shusta, E., & Ingber, D. E. (2019). Hypoxia-enhanced Blood-Brain
689 Barrier Chip recapitulates human barrier function and shuttling of drugs and antibodies. *Nature*
690 *Communications*, 1–12. https://doi.org/10.1038/s41467-019-10588-0

691 Chizhikov, V. V., Lindgren, A. G., Mishima, Y., Roberts, R. W., Aldinger, K. A., Miesegaes, G. R.,
692 Currle, D. S., Monuki, E. S., & Millen, K. J. (2010). Lmx1a regulates fates and location of cells

originating from the cerebellar rhombic lip and telencephalic cortical hem. *Proceedings of the National Academy of Sciences*. https://doi.org/10.1073/pnas.0910786107

Chizhikov, Victor V., & Millen, K. J. (2004). Mechanisms of roof plate formation in the vertebrate CNS. *Nature Reviews Neuroscience*, *5*(10), 808–812. https://doi.org/10.1038/nrn1520

Cornejo, I., Villanueva, S., Burgos, J., López-Cayuqueo, K. I., Chambrey, R., Julio-Kalajzic, F., Buelvas, N., Niemeyer, M. I., Figueiras-Fierro, D., Brown, P. D., Sepúlveda, F. V., & Cid, L. P. (2018). Tissue distribution of Kir7.1 inwardly rectifying K+ channel probed in a knock-in mouse expressing a haemagglutinin-tagged protein. *Frontiers in Physiology*, *9*(APR), 1–12. https://doi.org/10.3389/fphys.2018.00428

Culjat, M., & Milošević, N. J. (2019). Callosal septa express guidance cues and are paramedian guideposts for human corpus callosum development. *Journal of Anatomy*, *235*(3), 670–686. https://doi.org/10.1111/joa.13011

Dani, N., Herbst, R. H., Habib, N., Head, J., Dionne, D., Nguyen, L., Mccabe, C., Cui, J., Shipley, F. B., Jang, A., Rodman, C., Riesenfeld, S. J., Zhang, F., Rozenblatt-Rosen, O., Regev, A., & Lehtinen, M. K. (n.d.). *A cellular and spatial map of the choroid plexus across brain ventricles and ages*. https://doi.org/10.1101/627539

Dobin, A., Davis, C. A., Schlesinger, F., Drenkow, J., Zaleski, C., Jha, S., Batut, P., Chaisson, M., & Gingeras, T. R. (2013). STAR: Ultrafast universal RNA-seq aligner. *Bioinformatics*, *29*(1), 15–21. https://doi.org/10.1093/bioinformatics/bts635

Eiraku, M., Watanabe, K., Matsuo-Takasaki, M., Kawada, M., Yonemura, S., Matsumura, M., Wataya, T., Nishiyama, A., Muguruma, K., & Sasai, Y. (2008). Self-Organized Formation of Polarized Cortical Tissues from ESCs and Its Active Manipulation by Extrinsic Signals. *Cell Stem Cell*, *3*(5), 519–532. https://doi.org/10.1016/j.stem.2008.09.002

Ernst, S. A., Palacios, J. R., & Siegel, G. J. (1986). Immunocytochemical localization of Na+,K+-ATPase catalytic polypeptide in mouse choroid plexus. *Journal of Histochemistry and Cytochemistry*, *34*(2), 189–195. https://doi.org/10.1177/34.2.3003182

Furuta, Y., Piston, D. W. & Hogan, B. L. M. Bone morphogenetic proteins (BMPs) as regulators of dorsal forebrain development. *Development* **124**, 2203–2212 (1997).

Gao, C., Wang, Y., Broaddus, R., Sun, L., Xue, F., & Zhang, W. (2018). Exon 3 mutations of CTNNB1 drive tumorigenesis: A review. *Oncotarget*, *9*(4), 5492–5508. https://doi.org/10.18632/oncotarget.23695

724 Grove, E. A., Tole, S., Limon, J., Yip, L. W., & Ragsdale, C. W. (1998). The hem of the embryonic
725 cerebral cortex is defined by the expression of multiple Wnt genes and is compromised in Gli3-
726 deficient mice. *Development*, *125*(12), 2315–2325.

727 Gu, X., Liu, B., Wu, X., Yan, Y., Zhang, Y., Wei, Y., Pleasure, S. J., & Zhao, C. (2011). Inducible
728 genetic lineage tracing of cortical hem derived Cajal-Retzius cells reveals novel properties. *PLoS*
729 *ONE*. https://doi.org/10.1371/journal.pone.0028653

730 Harada, N., Tamai, Y., Ishikawa, T. O., Sauer, B., Takaku, K., Oshima, M., & Taketo, M. M. (1999).
731 Intestinal polyposis in mice with a dominant stable mutation of the β-catenin gene. *EMBO*
732 *Journal*, *18*(21), 5931–5942. https://doi.org/10.1093/emboj/18.21.5931

733 Hébert, J. M., Mishina, Y., & McConnell, S. K. (2002). BMP signaling is required locally to pattern
734 the dorsal telencephalic midline. *Neuron*, *35*(6), 1029–1041. https://doi.org/10.1016/S0896-
735 6273(02)00900-5

736 Huelsken, J., Vogel, R., Erdmann, B., Cotsarelis, G., & Birchmeier, W. (2001). β-Catenin controls
737 hair follicle morphogenesis and stem cell differentiation in the skin. *Cell*, *105*(4), 533–545.
738 https://doi.org/10.1016/S0092-8674(01)00336-1

739 Imayoshi, I., Shimogori, T., Ohtsuka, T., & Kageyama, R. (2008). Hes genes and neurogenin
740 regulate non-neural versus neural fate specification in the dorsal telencephalic midline.
741 *Development*. https://doi.org/10.1242/dev.021535

742 Johansson, P. A., Irmler, M., Acampora, D., Beckers, J., Simeone, A., & Gotz, M. (2013). The
743 transcription factor Otx2 regulates choroid plexus development and function. *Development*,
744 *140*(5), 1055–1066. https://doi.org/10.1242/dev.090860

745 Johansson, Pia A. (2014). The choroid plexuses and their impact on developmental
746 neurogenesis. *Frontiers in Neuroscience*, *8*(OCT), 1–9. https://doi.org/10.3389/fnins.2014.00340

747 Kajino, Y., Yamaguchi, A., Hashimoto, N., Matsuura, A., Sato, N., & Kikuchi, K. (2001). β-Catenin
748 gene mutation in human hair follicle-related tumors. *Pathology International*, *51*(7), 543–548.
749 https://doi.org/10.1046/j.1440-1827.2001.01231.x

750 Karzbrun, E., Kshirsagar, A., Cohen, S. R., Hanna, J. H., & Reiner, O. (2018). Human brain
751 organoids on a chip reveal the physics of folding. *Nature Physics*, *14*(5), 515–522.
752 https://doi.org/10.1038/s41567-018-0046-7

753 Kemler, R., Hierholzer, A., Kanzler, B., Kuppig, S., Hansen, K., Taketo, M. M., de Vries, W. N.,
754 Knowles, B. B., & Solter, D. (2004). Stabilization of β-catenin in the mouse zygote leads to

755 premature epithelial-mesenchymal transition in the epiblast. *Development*, *131*(23), 5817–
756 5824. https://doi.org/10.1242/dev.01458

757 Kim, D., Paggi, J. M., Park, C., Bennett, C., & Salzberg, S. L. (2019). Graph-based genome
758 alignment and genotyping with HISAT2 and HISAT-genotype. *Nature Biotechnology*, *37*(8), 907–
759 915. https://doi.org/10.1038/s41587-019-0201-4

760 Kim, H., Wu, J., Ye, S., Tai, C. I., Zhou, X., Yan, H., Li, P., Pera, M., & Ying, Q. L. (2013). Modulation
761 of β-catenin function maintains mouse epiblast stem cell and human embryonic stem cell self-
762 renewal. *Nature Communications*, *4*(61). https://doi.org/10.1038/ncomms3403

763 Kim, J., & Jung, Y. (2012). Increased aquaporin-1 and Na+-K+-2Cl-cotransporter 1 expression in
764 choroid plexus leads to blood-cerebrospinal fluid barrier disruption and necrosis of
765 hippocampal CA1 cells in acute rat models of hyponatremia. *Journal of Neuroscience Research*,
766 *90*(7), 1437–1444. https://doi.org/10.1002/jnr.23017

767 Kim, S., & Jeong, S. (2019). Mutation hotspots in the β-catenin gene: Lessons from the human
768 cancer genome databases. *Molecules and Cells*, *42*(1), 8–16.
769 https://doi.org/10.14348/molcells.2018.0436

770 Konno, D., Iwashita, M., Satoh, Y., Momiyama, A., Abe, T., Kiyonari, H., & Matsuzaki, F. (2012).
771 The Mammalian DM Domain Transcription Factor Dmrta2 Is Required for Early Embryonic
772 Development of the Cerebral Cortex. *PLoS ONE*, *7*(10), 1–13.
773 https://doi.org/10.1371/journal.pone.0046577

774 Langford, M. B., O'Leary, C. J., Veeraval, L., White, A., Lanoue, V., & Cooper, H. M. (2020).
775 WNT5a Regulates Epithelial Morphogenesis in the Developing Choroid Plexus. *Cerebral Cortex*.
776 https://doi.org/10.1093/cercor/bhz330

777 Lee, S. M., Tole, S., Grove, E., & McMahon, a P. (2000). A local Wnt-3a signal is required for
778 development of the mammalian hippocampus. *Development*, *127*(3), 457–467.

779 Li, C., Li, A., Xing, Y., Li, M., Chan, B., Ouyang, R., Taketo, M. M., Kucherlapati, R., Borok, Z., &
780 Minoo, P. (2013). Apc deficiency alters pulmonary epithelial cell fate and inhibits Nkx2.1 via
781 triggering TGF-beta signaling. *Developmental Biology*, *378*(1), 13–24.
782 https://doi.org/10.1016/j.ydbio.2013.03.018

783 Li, L., Grausam, K. B., Wang, J., Lun, M. P., Ohli, J., Lidov, H. G. W., Calicchio, M. L., Zeng, E.,
784 Salisbury, J. L., Wechsler-Reya, R. J., Lehtinen, M. K., Schüller, U., & Zhao, H. (2016). Sonic
785 Hedgehog promotes proliferation of Notch-dependent monociliated choroid plexus tumour
786 cells. *Nature Cell Biology*, *18*(4), 418–430. https://doi.org/10.1038/ncb3327

Liddelow, S. A., Dziegielewska, K. M., VandeBerg, J. L., & Saunders, N. R. (2010). Development of the lateral ventricular choroid plexus in a marsupial, Monodelphis domestica. *Cerebrospinal Fluid Research*, *7*, 1–10. https://doi.org/10.1186/1743-8454-7-16

Louvi, A., Yoshida, M., & Grove, E. A. (2007). The derivatives of the Wnt3a lineage in the central nervous system. *Journal of Comparative Neurology*, *504*(5), 550–569. https://doi.org/10.1002/CNE.21461

Love, M. I., Huber, W., & Anders, S. (2014). Moderated estimation of fold change and dispersion for RNA-seq data with DESeq2. *Genome Biology*, *15*(12), 1–21. https://doi.org/10.1186/s13059-014-0550-8

Lun, M. P., Johnson, M. B., Broadbelt, K. G., Watanabe, M., Kang, Y. J., Chau, K. F., Springel, M. W., Malesz, A., Sousa, A. M. M., Pletikos, M., Adelita, T., Calicchio, M. L., Zhang, Y., Holtzman, M. J., Lidov, H. G. W., Sestan, N., Steen, H., Monuki, E. S., & Lehtinen, M. K. (2015). Spatially heterogeneous choroid plexus transcriptomes encode positional identity and contribute to regional CSF production. *Journal of Neuroscience*, *35*(12), 4903–4916. https://doi.org/10.1523/JNEUROSCI.3081-14.2015

Machon, O., Backman, M., Machonova, O., Kozmik, Z., Vacik, T., Andersen, L., & Krauss, S. (2007). A dynamic gradient of Wnt signaling controls initiation of neurogenesis in the mammalian cortex and cellular specification in the hippocampus. *Developmental Biology*, *311*(1), 223–237. https://doi.org/10.1016/j.ydbio.2007.08.038

Mangale, V. S., Hirokawa, K. E., Satyaki, P. R. V., Gokulchandran, N., Chikbire, S., Subramanian, L., Shetty, A. S., Martynoga, B., Paul, J., Mai, M. V., Li, Y., Flanagan, L. A., Tole, S., & Monuki, E. S. (2008). Lhx2 selector activity specifies cortical identity and suppresses hippocampal organizer fate. *Science*, *319*(5861), 304–309. https://doi.org/10.1126/science.1151695

MARTIN, Marcel. Cutadapt removes adapter sequences from high-throughput sequencing reads. EMBnet.journal, [S.l.], v. 17, n. 1, p. pp. 10-12, may 2011. ISSN 2226-6089. Available at: <https://journal.embnet.org/index.php/embnetjournal/article/view/200/479>. Date accessed: 21 nov. 2020. doi:https://doi.org/10.14806/ej.17.1.200.

Meador, J. P., Lech, J. J., Rice, S. D., Hose, J. E., Short, J. W., Rice, S. D., Collier, T. K., Scholz, N. L., Collier, T. K., Scholz, N. L., Campana, S. E., Carlsson, L., Duker, G., Kass, R. S., Roden, D. M., Darbar, D., Cheng, H., Lederer, W. J., Freund, E. V, … White, E. (2014). Science Volume 343 issue 6172 2014 [doi 10.1126%2Fscience.1247651] Jaitin, D. A.; Kenigsberg, E.; Keren-Shaul, H.; Elefant, N.; Pau -- Massively Parallel Single-Cell RNA-Seq for Marker-Free Decomposit.pdf. February.

820 Meeker, R. B., Williams, K., Killebrew, D. A. & Hudson, L. C. Cell trafficking through the choroid
821 plexus. *Cell Adhes. Migr.* **6**, 390–396 (2012).

822 Monuki, E. S., Porter, F. D., & Walsh, C. A. (2001). *Monuki ES, 2001.pdf*. *32*, 591–604.

823 Pellegrini, L., Bonfio, C., Chadwick, J., Begum, F., Skehel, M., & Lancaster, M. A. (2020). Human
824 CNS barrier-forming organoids with cerebrospinal fluid production. *Science*, *369*(6500), 1–21.
825 https://doi.org/10.1126/science.aaz5626

826 Sakaguchi, H., Kadoshima, T., Soen, M., Narii, N., Ishida, Y., Ohgushi, M., Takahashi, J., Eiraku,
827 M., & Sasai, Y. (2015). Generation of functional hippocampal neurons from self-organizing
828 human embryonic stem cell-derived dorsomedial telencephalic tissue. *Nature Communications*.
829 https://doi.org/10.1038/ncomms9896

830 Saunders, N. R., Dziegielewska, K. M., Møllgård, K., Habgood, M. D., Wakefield, M. J., Lindsay,
831 H., Stratzielle, N., Ghersi-Egea, J. F., & Liddelow, S. A. (2015). Influx mechanisms in the
832 embryonic and adult rat choroid plexus: A transcriptome study. *Frontiers in Neuroscience*,
833 *9*(MAR). https://doi.org/10.3389/fnins.2015.00123

834 Solberg, N., Machon, O., & Krauss, S. (2008). Effect of canonical Wnt inhibition in the
835 neurogenic cortex, hippocampus, and premigratory dentate gyrus progenitor pool.
836 *Developmental Dynamics*, *237*(7), 1799–1811. https://doi.org/10.1002/dvdy.21586

837 Speake, T., Kibble, J. D., & Brown, P. D. (2004). Kv1.1 and Kv1.3 channels contribute to the
838 delayed-rectifying K + conductance in rat choroid plexus epithelial cells. *American Journal of*
839 *Physiology - Cell Physiology*, *286*(3 55-3), 611–620. https://doi.org/10.1152/ajpcell.00292.2003

840 Steffensen, A. B., Oernbo, E. K., Stoica, A., Gerkau, N. J., Barbuskaite, D., Tritsaris, K., Rose, C. R.,
841 & MacAulay, N. (2018). Cotransporter-mediated water transport underlying cerebrospinal fluid
842 formation. *Nature Communications*, *9*(1), 1–13. https://doi.org/10.1038/s41467-018-04677-9

843 Supek, F., Bošnjak, M., Škunca, N., & Šmuc, T. (2011). Revigo summarizes and visualizes long
844 lists of gene ontology terms. *PLoS ONE*, *6*(7). https://doi.org/10.1371/journal.pone.0021800

845 Wang, Y., Sabbagh, M. F., Gu, X., Rattner, A., Williams, J., & Nathans, J. (2019). Beta-catenin
846 signaling regulates barrier-specific gene expression in circumventricular organ and ocular
847 vasculatures. *ELife*, 1–36. https://doi.org/10.7554/eLife.43257

848 Watanabe, M., Kang, Y., Davies, L. M., Meghpara, S., Lau, K., Chung, C., Kathiriya, J.,
849 Hadjantonakis, A., & Monuki, E. S. (2012). *BMP4 Sufficiency to Induce Choroid Plexus Epithelial*
850 *Fate from Embryonic Stem Cell-Derived Neuroepithelial Progenitors*. *32*(45), 15934–15945.

https://doi.org/10.1523/JNEUROSCI.3227-12.2012

Ying, Q. L., Wray, J., Nichols, J., Batlle-Morera, L., Doble, B., Woodgett, J., Cohen, P., & Smith, A. (2008). The ground state of embryonic stem cell self-renewal. *Nature*, *453*(7194), 519–523. https://doi.org/10.1038/nature06968

Yoshida, M. (2006). Massive loss of Cajal-Retzius cells does not disrupt neocortical layer order. *Development*, *133*(3), 537–545. https://doi.org/10.1242/dev.02209

Yu, G., Wang, L. G., Han, Y., & He, Q. Y. (2012). ClusterProfiler: An R package for comparing biological themes among gene clusters. OMICS A Journal of Integrative Biology, 16(5), 284–287. https://doi.org/10.1089/omi.2011.0118

Zappaterra, M. W., & Lehtinen, M. K. (2012). The cerebrospinal fluid: Regulator of neurogenesis, behavior, and beyond. *Cellular and Molecular Life Sciences*, *69*(17), 2863–2878. https://doi.org/10.1007/s00018-012-0957-x

Zhao Y, Sheng HZ, Amini R, Grinberg A, Lee E, Huang S, Taira M, Westphal H. Control of hippocampal morphogenesis and neuronal differentiation by the LIM homeobox gene Lhx5. Science. 1999; 284:1155–1158